Biomacromolecules

Subscriber access provided by GRIFFITH UNIVERSITY

Article

H-Ferritin Enriches the Curcumin Uptake and Improves the Therapeutic Efficacy in Triple Negative Breast Cancer Cells

Laura Pandolfi, Michela Bellini, Renzo Vanna, Carlo Morasso, Andrea Zago, Sofia Carcano, Svetlana Avvakumova, Jessica Armida Bertolini, Maria Antonietta Rizzuto, Miriam Colombo, and Davide Prosperi

Biomacromolecules, **Just Accepted Manuscript** • DOI: 10.1021/acs.biomac.7b00974 • Publication Date (Web): 08 Sep 2017

ACS Publications

Biomacromolecules is published by the American Chemical Society. 1155 Sixteenth Street N.W., Washington, DC 20036

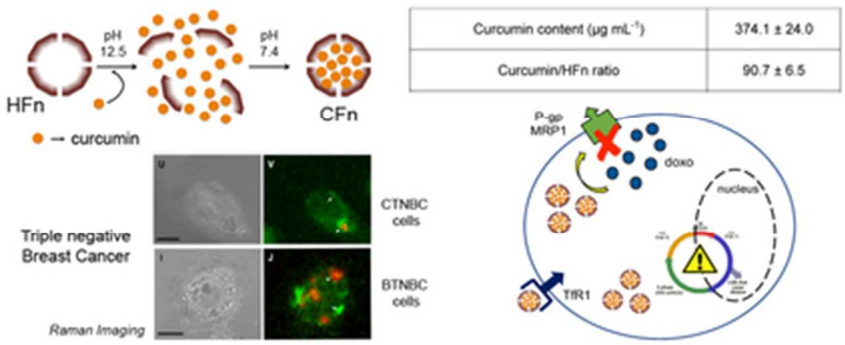

Graphical Abstract

35x14mm (300 x 300 DPI)

H-Ferritin Enriches the Curcumin Uptake and Improves the Therapeutic Efficacy in Triple Negative Breast Cancer Cells

Laura Pandolfi,[¶,‡] *Michela Bellini,*[¶,‡] *Renzo Vanna,*[†] *Carlo Morasso,*[†] *Andrea Zago,*[¶] *Sofia Carcano,*[¶] *Svetlana Avvakumova,*[¶] *Jessica Armida Bertolini,*[¶] *Maria Antonietta Rizzuto,*[¶] *Miriam Colombo,*[¶] *Davide Prosperi*[¶,*]

[¶]NanoBioLab, Dipartimento di Biotecnologie e Bioscienze, Università di Milano-Bicocca, 20126 Milano, Italy; [†]LABION, Fondazione Don Carlo Gnocchi ONLUS, Piazzale Morandi 6, 20121 Milan, Italy.

KEYWORDS: curcumin; biomimetic nanoparticles; ferritin; triple negative breast cancer; chemotherapy.

Triple negative breast cancer (TNBC) is a highly aggressive, invasive and metastatic tumor. Although it is reported to be sensitive to cytotoxic chemotherapeutics, frequent relapse and chemoresistance often result in treatment failure. In this study, we developed a biomimetic nanodrug consisting of a self-assembling variant (HFn) of human apoferritin loaded with curcumin. HFn nanocage improved the solubility, chemical stability, and bioavailability of curcumin, allowing us to reliably carry out several experiments in the attempt to establish the

potential of this molecule as a therapeutic agent and elucidate the mechanism of action in TNBC. HFn biopolymer was designed to bind selectively to the TfR1 receptor overexpressed in TNBC cells. HFn-curcumin (CFn) proved to be more effective in viability assays compared to the drug alone using MDA-MB-468 and MDA-MB-231 cell lines, representative of basal and claudin-low TNBC subtypes, respectively. Cellular uptake of CFn was demonstrated by flow cytometry and label-free confocal Raman imaging. CFn could act as a chemosensitizer enhancing the cytotoxic effect of doxorubicin by interfering with the activity of multidrug resistance transporters. In addition, CFn exhibited different cell cycle effects on these two TNBC cell lines, blocking MDA-MB-231 in G0/G1 phase whereas MDA-MB-468 accumulated in G2/M phase. CFn was able to inhibit the Akt phosphorylation, suggesting that the effect on the proliferation and cell cycle involved the alteration of PI3K/Akt pathway.

INTRODUCTION

Breast cancer (BC) is a very complex disease characterized by heterogeneous morphological features and unrelated clinical behavior. In the past decades, BC was classified basing on immunohistochemistry, tumor grade, lymph nodes status and, more recently, on predictive panel markers, particularly related to the extent of expression of specific genes, including progesterone (PR), estrogen (ER) and human epidermal growth factor 2 (HER-2) receptors.[1,2] Five BC subtypes have been identified depending on the molecular profiling, namely luminal A, luminal B, HER2, basal and claudin-low.[3] The existence of a therapeutic target normally determines the choice of the therapeutic approach to BC, thus luminal A and luminal B are treated by hormone therapy whereas tumors with HER2/Neu gene amplification are candidates for trastuzumab.[4] As

basal group phenotype lacks the expression of all of these three receptors, it is usually referred to as "triple negative" breast cancer (TNBC). However, TNBC is a broader definition encompassing different subtypes, most frequently basal and claudin-low. The latter is characterized not only by the lack of PR, ER and HER2, but also by low expression of claudins and Ki67 marker of proliferation, enhancement of epithelial-mesenchymal transition and stem cell features, generally leading to poor prognosis.[5] Although TNBC represents only the 15% of BCs in women, it is associated to highly aggressive nature and metastatic development with very common relapse and median survival around 13 months.[6] TNBCs are usually sensitive to anthracyclines and taxanes,[7] which are part of the standard therapy used for high-risk patients, while cisplatin has shown encouraging effects in patients with BRCA1 mutation (*ca.* 10% of TNBC tumors).[2] In addition, anti-angiogenic agents, including bevacizumab, sunitinib and sorafenib, or newer targeted therapies using monoclonal antibodies, such as cetuximab, proved sometimes beneficial in combination therapy.[8,9] However, complete response does not correlate with overall survival. Frequent relapse and chemoresistance in TNBCs are attributable to the ability of these cancer cells to bypass the apoptotic mechanisms through the activation of alternative pathways, including cellular senescence or cytoprotective autophagy.[10] This dramatic picture suggests that an unmet need for improved agents is demanded for patients affected by TNBC.

Turmeric (*Curcuma longa L.*) has long been used in Indian medicine for the treatment of several life-threatening diseases.[11] The medicinal properties of this plant have been attributed to the diferuloylmethane ($C_{21}H_{20}O_6$), an insoluble yellow powder commonly referred to as curcumin, which is the main component of the rhizome. This compound was found to possess a wide range of pharmacological activities, including anti-inflammatory, antioxidant and

antitumor, providing additional benefits for many diseases, including neurodegenerative disorders (*e.g.*, Alzheimer's disease), cardiovascular diseases and diabetes.[12] Curcumin is able to interfere with multiple signaling pathways affecting proliferation, apoptosis, inflammation and angiogenesis in tumors. Given the multifactoriality of cancer, the pleiotropic activity of curcumin has attracted great expectation making it a promising candidate for the treatment of a broad range of aggressive cancer subtypes.[13,14]

Even if several publications and a few clinical trials have demonstrated the great potential of curcumin in influencing numerous signaling and metabolic pathways at the cellular level,[15] this molecule has not been approved as a therapeutic agent because of a few limitations. Indeed, curcumin has poor solubility in water and is susceptible to fast degradation. In addition, the reliability of the activity assays with curcumin and its metabolites have been recently questioned due to low molecular stability and to the optical properties of the unsaturated system that could interfere with most analytical assays, raising doubts on the actual therapeutic potential of this molecule suggested by those experiments.[16] *In vivo* studies related to absorption, distribution, metabolism, and excretion (ADME) revealed extremely rapid metabolism and poor absorption of this molecule, which severely reduce its bioavailability.[17,18] Several approaches were attempted to improve the bioavailability, to increase the plasma concentration, and to enhance the cellular permeability and resistance to metabolic processes of curcumin, including 1) the use of adjuvants to block curcumin metabolism;[19] 2) the synthesis of curcumin analogues altering the chemical structure;[20,21] and 3) nanoformulation.[22,23] In a previous work, we showed that incorporating curcumin in polylactic-*co*-glycolic (PLGA) nanoparticles improved the chemical stability of the drug within the cellular environment, which increased the antiproliferative effect of curcumin against estrogen-dependent MCF-7 BC cells.[24] That work, together with other numerous *in vitro*

and *in vivo* studies, suggested that nanoformulation of curcumin is a favorable option to control and enhance the potential of this molecule. An additional advantage in the use of nanoparticles is that they allow the drug to be selectively targeted to cell subtypes taking advantage of an established technology for the functionalization of their surface with ligands directed to specific cellular receptors.[25]

In the present work, we developed a novel method for the incorporation of curcumin in H-ferritin (HFn), a biomimetic nanoparticle consisting in a recombinant protein complex composed of 24 identical heavy chain subunits of human apoferritin, which self-assemble into a spherical cage of 12 nm having an internal cavity around 8 nm.[26] A convenient feature of this globular protein is that HFn shell is unfolded into individual subunits at strongly acidic (*i.e.*, below 3) or alkaline (around 11-12) pHs and refolds into the original quaternary structure with perfect shape memory when the pH neutrality of the solution is restored.[27,28] This aptitude allowed the easy incorporation of drugs into the nanocage cavity, making HFn a valuable nanocarrier for a variety of active molecules or inorganic cores useful for therapeutic or imaging purposes.[29] Notably, Li *et al.* reported that HFn is recognized with high affinity by the transferrin receptor 1 (TfR1) and this binding resulted in the clathrin-dependent cellular uptake of HFn into endosomes and lysosomes.[30] In a recent study, the TfR1 receptor was found overexpressed in 98% primary and metastatic human solid tumors, whereas it was downregulated in the relevant healthy tissues.[31] The upregulation of the TfR1 gene in malignant cells, its ability to be internalized, and the enhanced need of iron for cancer cell proliferation make this receptor a widely accessible portal of entry for cytotoxic drugs into malignant cells and indicate HFn nanocages as an attractive targeted delivery system for cancer therapy.[32]

In this study, we aimed to exploit the pH sensitivity of HFn to encapsulate curcumin in order to improve the chemical stability of the drug in a biological environment and exploit the specific binding to TfR1 to enrich the drug accumulation in TNBC cells. We assessed the biological activity of HFn-curcumin (CFn) compared to curcumin alone (dissolved in dimethyl sulfoxide, DMSO) using two different TNBC cell lines, namely MDA-MB-468 and MDA-MB-231, belonging to the basal and claudin-low BC subtypes, respectively.

MATERIALS AND METHODS

Curcumin purification. Commercially available curcumin from *Curcuma longa* (powder, Sigma Aldrich) generally contains other curcuminoids, like demethoxycurcumin and bisdemethoxycurcumin, as secondary products.[12] However, it is possible to separate the three curcuminoids using crystallization and column chromatography.[33] The dark yellow powder purchased from Sigma Aldrich was purified by column chromatography on silica gel, choosing as mobile phase a mixture of chloroform and methanol (98:2). After elution, the purity of the fractions containing curcumin was assessed by thin-layer chromathography (TLC), using the same mobile phase (Figure S1). Fractions containing the product of interest were collected and evaporated under reduced pressure.

HFn nanocage design and purification from *E. Coli.* The cDNA encoding for the heavy chain of human ferritin, modified by inserting the restriction sites for NdeI and NotI (respectively in 5' and 3'), was synthesized and subcloned into the vector pET30b(+) by Eurofins MWG Operon to express HFn under the control of a T7 promoter, as reported in Bellini *et al.*[28] The resulting plasmid pET30b/HFn was used to transform *Escherichia coli* expression strain

BL21(DE3) by heat-shock method. The recombinant expression vector was confirmed by restriction endonuclease digestion and DNA sequencing. HFn was expressed and purified following the protocol previously published.[28] Briefly, BL21(DE3)/pET30b/HFn cell were grown at 37 °C in Luria Bertani kanamicim medium until OD_{600} = 0.6 and induced with 0.5 mM isopropyl β-D-1-tiogalactopiranoside (IPTG) for 2.5 h. After growing, the cells were collected, washed and resuspended in lysis buffer with lysozyme and DNase I. In order to prepare the crude extract, cells were sonicated, centrifuged and heated at 70 °C. The supernatant was loaded onto DEAE sepharose anion exchange resin, and the purified protein was eluted with a stepwise NaCl gradient in 20 mM KMES, pH 6.0. Fractions were analyzed by SDS-PAGE using 12% (v/v) polyacrylamide gel and proteins were detected with Coomassie blue staining. Protein content was determined by both measuring absorbance at 280 nm and Coomassie Plus Protein Assay Reagent (Thermo Fisher Scientific) with IgG as standard protein.

HFn loading with curcumin (CFn). Encapsulation of Cur inside the HFn cavity was achieved exploiting a disassembly/reassembly strategy. The pH of a HFn solution (1 mg mL^{-1} in 0.15 M NaCl) was adjusted to 12.5 by adding the appropriate volume of 1 M NaOH. After 15 min, a 400 μM solution of purified Cur, freshly solubilized in 0.1 M sodium hydroxide, was added. Immediately, the pH value was lowered to 7.5 using 1 M HCl. The resulting solution was stirred at room temperature for 2 h to promote the assembly of the protein. Later, the solution was centrifuged through a 100 kDa Amicon filter (Millipore), washed several times with sterile PBS buffer and finally refined on Zeba™ Spin Desalting Columns (Thermo Scientific), in order to remove the excess Cur and the adsorbed molecules. The encapsulated Cur was supposed to be retained inside the apoferritin shell because its size is larger than the pore size of the protein channels (3–4 Å),[34] while the excess molecules were assumed to be removed in the washing

steps. The final product that we termed CFn was subsequently characterized and used for *in vitro* experiments. To evaluate the intracellular fate of CFn, the HFn shell was also labeled with fluorescein isothiocyanate (FITC) according to the manufacturer's protocol (Sigma, Invitrogen).

Determination of the loading efficiency. The number of encapsulated molecules was determined comparing the absorbance intensity at 423 nm of different CFn dilutions in acetic acid with a predetermined Cur calibration curve using EnSight™ Multimode Plate Reader (Perkin Elmer®). After suspending CFn in acetic acid, the pH of the samples was reduced to 2.0, allowing the encapsulated Cur to be released from ferritin. In order to get a calibration curve (Figure S2), individual working standard solutions of purified Cur (from 1 to 95 μM) were freshly prepared from Cur stock standard solution by diluting in acetic acid.

Curcumin stability. CFn was characterized analyzing its stability in solution under physiologic and alkaline conditions, in comparison with a free Cur in solution. CFn or Cur were suspended in phosphate buffer saline (PBS, pH 7.2) and sodium hydroxide (0.1 M NaOH, pH 12.5), at 50 μM final concentration. Since Cur is fairly soluble in alkaline solution but poorly soluble in water, purified Cur was dissolved in DMSO at 50 mM and then diluted in PBS buffer for the stability experiments at neutral pH. The final concentration of DMSO in solution was negligible. At predetermined time points (30 min, 1, 2, 3, 4, 5, 6, 24, and 48 h), an aliquot of each solution was transferred into a cuvette and the absorption spectrum was analyzed by NanoDrop 2000c UV-Vis Spectrophotometer (Thermo Scientific). The average of three different samples at each time point was used to evaluate the stability of the solution over time.

TEM, DLS analysis. To check the morphology of CFn, the nanocages were analyzed by transmission electron microscopy (TEM). For the analysis, a sample of a CFn solution was

dropped onto the surface of a copper net and stained with 2% phosphotungstic acid for 10 min. The nanoparticle structure was directly observed using Tecnai™ G2 Spirit BioTWIN (FEI) TEM at 120 K after drying the samples at room temperature for 2 h. For dynamic light scattering (DLS) experiments, CFn nanoparticles and Cur were suspended in PBS, pH 7.2, at a final concentration of 50 μM Cur.

Native electrophoresis gel. For native PAGE of HFn and CFn, recombinant HFn (5 μg) and CFn nanoparticles were loaded onto PAGE (6% acrylamide) under native conditions to evaluate quaternary structure formation and visualized by Coomassie staining (Figure S6).

Raman spectroscopy and confocal Raman imaging. Raman spectra were recorded using an Aramis micro-Raman from Horiba Jobin-Yvon equipped with laser light sources operating at 633 and 785 nm. The Raman spectrometer was calibrated daily using different bands of cyclohexane (*i.e.*, 801.3, 1266.4 nd 1444.4 cm^{-1}). Raman spectra of free Cur and CFn were acquired on a small amount of sample dried from water on a CaF_2 slide (Crystran, UK) without any further preparation. Spectra were collected using a 785-nm laser line of 125 mW focused on the sample using a 50× objective for 20 seconds. Shown spectra are the averaging of 4 different acquisitions after baseline subtraction. Raman spectra relative to CFn stability are taken on a suspension of nanoparticles in PBS using a 785-nm laser line of 250 mW focused on a 50 μL drop of suspension using a 20× objective for 120 seconds. Shown spectra are the averaging of 3 different acquisitions after baseline subtraction. Before Raman imaging experiments 1.5×10^5 CTNBC or BTNBC were seeded on CaF_2 discs previously treated with poly-lysine 0.01% overnight at 4 °C. Cells were grown for 24 h and then incubated for 15 min, 4 h, or 24 h at 37 °C with CFn 20 μM. Cells were then washed with PBS and fixed with 2% PFA in PBS for 30 min at 37 °C. Confocal Raman images were acquired directly in PBS by coupling the 633 He-Ne laser

(source power 17 mW) with an immersion objective (63×/1.0 NA, Zaiss). Cells were scanned with 0.8 μm step-size by acquiring 2.3 seconds ×2 for each step at 3.0 μm above the optical substrate. Bright field images were acquired just after each measurement. LabSpec6 software (HORIBA scientific) was used to produce Raman images (univariate imaging and classical least square (CLS) fitting) and for RGB manipulation. The average spectrum of the surface not covered by cells was subtracted from each imaging dataset in order to remove the background signal (mostly CaF_2 substrate and water). No further baseline correction or noise removal post-processing have been performed to imaging dataset. OriginLab2017 was used to process and to plot the representative spectra.

Cell cultures. MDA-MB-231 (claudin-low subtype, CTNBC) and MDA-MB-468 (basal subtype, BTNBC) cell lines were cultured in Minimum Essential Media (MEM) and Dulbecco's Modified Eagle's Medium (DMEM), respectively, supplemented with 10% fetal bovine serum (FBS), 2 mM L-glutamine, penicillin (50 UI mL^{-1}) and streptomycin (50 mg mL^{-1}) at 37 °C in humidified atmosphere containing 5% CO_2 and sub-cultured prior to confluence using trypsin/EDTA. Cell culture medium, supplements and antibiotics were purchased by EuroClone.

Interaction of CFn with TNBC cells. For cellular uptake analysis, CTNBC and BTNBC were plated at a density of 3×10^5 in 12-wells and after 24 h at 37 °C were incubated with 50 μg mL^{-1} of CFn and HFn labeled with FITC (CFn-FITC and HFn-FITC, respectively) for 15 min, 1, 4, 24, 48 and 72 h at 37 °C. For the binding assay, CTNBC and BTNBC were harvested (3×10^5 cells) in FACS tubes. After centrifugation, cells were washed with PBS/1% BSA solution and incubated for 2 h at 4 °C with CFn (50 μg mL^{-1}) labeled with FITC in PBS/1% BSA. After the incubation times, the cells were washed and analyzed by Gallios™ Flow Cytometer (Beckman

Coulter Inc.). The mean fluorescence intensity of Cur and FITC signals was analyzed acquiring 10000 events per sample. Data were expressed as mean ± standard deviation (SD) of three independent replicates.

Viability assay. To test CFn and Cur toxicity, MTT assay (CellTiter 96 Non-Radioactive cell proliferation assay, Promega) was performed. Cells (10^3) were seeded in a 96-wells plate, five replicates per each concentration. 24 h after plating, the two cell lines were treated for 24, 48 and 72 h with 5, 10, 20, 35 and 50 μM Cur and CFn. CFn amount was estimated on the basis of its Cur content in order to compare the concentration of Cur encapsulated inside nanocages with free molecule. According to the manufacturer's instructions, at the end of the exposure time, MTT was added and formazan product was detected after 4 h at 37 °C reading the absorbance at 570 nm with EnSight™ Multimode Plate Reader (Perkin Elmer®) subtracting the absorbance of background at 620 nm. Results were obtained normalizing by the untreated control and expressed as percentage ± standard deviation of three independent biological replicates.

Assessment of TNBC chemoresistance. We assessed the presence of multidrug resistance related to the activity of two major ABC transporter proteins using a specific assay kit (EFFLUX-ID Gold multidrug resistance assay kit, Enzo Life Science Inc.). CTNBC and BTNBC (5×10^5 cells) were collected in FACS tubes, centrifuged and resuspended with P-gp (Verapamil) and MRP-1 (MK571) inhibitors diluted in DMEM without phenol red. After 5 min at 37 °C, the non-fluorescent compound was added to each sample, where it readily penetrated the cell membrane and hydrolyzed to a hydrophilic fluorescent dye by intracellular esterases. After 30 min at 37 °C, cells where analyzed by flow cytometry quantifying the fluorescence of the

compound within the cells. The use of specific inhibitors for MDR proteins should give higher fluorescence intensity affording the measurement of the activity of each MDR protein.

For MDR protein efflux analysis, TNBC cells were plated at 3×10^4 cells in 96-well plate. After 24 h, cells were incubated with 1 μg mL^{-1} Rhodamine 6G (R6G) for 1 h at 37 °C allowing the accumulation of fluorescent molecules inside cells. After the incubation, cells were washed with PBS to eliminate the excess and treated with 20 μM CFn or free Cur. At different time points (30, 60, 90, 120, 150, 180 min, 6 and 24 h) the fluorescent intensity of released R6G in supernatants was read by Ensight multimode plate reader (Perkin Elmer) setting the λ_{ex} = 528 nm and λ_{em} = 550 nm. Data were represented as mean ± standard deviation of three replicates for all conditions.

Treatment of cells combining doxorubicin and CFn. To evaluate the effect of our nanoconstruct on sensitization of TNBC cells to doxorubicin treatment, we used an MTT assay. CTNBC and BTNBC (10^3 cells) were seeded in a 96-wells plate and subjected to five replicates per concentration. 24 h after plating, cells were treated for 24, 48 and 72 h with 0.1, 0.5, 1, 2.5, 5, 7.5 μM doxorubicin (Dox) in order to evaluate the cytotoxicity of the anthracycline. To analyze the enhancement of cell sensitivity to Dox treatments by CFn and Cur, we combined the range of Dox tested with 5, 10 and 20 μM CFn or free Cur, respectively, for 24, 48 and 72 h. According to the manufacturer's instructions, at the end of the exposure, MTT was added and formazan product was detected after 4 h at 37 °C reading the absorbance at 570 nm with EnSight™ Multimode Plate Reader (Perkin Elmer®) subtracting the background absorbance at 620 nm. Data were obtained normalizing the results with untreated control and were expressed as percentage ± standard deviation of three independent biological replicates.

Cell cycle analysis. CTNBC and BTNBC cells were seeded in a 12-wells plate (3×10^5 cells per well) and after 24 h were incubated with 5, 10 and 20 μM purified Cur or CFn for 48 h at 37 °C. Once collected and fixed in 70% ethanol, cellular DNA was stained with a mixture of propidium iodide (10 μg mL^{-1}) and RNase A (20 μg mL^{-1}). 10000 events for each sample were acquired using flow cytometry equipped with a doublet discriminator module (Gallios™ Flow Cytometer - Beckman Coulter Inc.), and the DNA content was analyzed by FlowJo software (TreeStar Inc., OR, U.S.A.).

Quantification of Akt phosphorylation by Alpha Technology. To quantify the decrease of Akt phosphorylation, we used the AlphaScreen® SureFire® p-Akt 1/2/3 (Ser 473) assay (Perkin Elmer), a sandwich immunoassay for quantitative detection of specific proteins in cellular lysates using Alpha Technology. CTNBC and BTNBC cells were seeded in a 96-wells plate (20×10^4 cells per well) and after 24 h were incubated with 20 μM purified Cur or CFn for 4 and 24 h at 37 °C. After incubation, the AlphaScreen® SureFire® was carried out according to the manufacterer's instruction. Briefly, cells were lysed with lysis buffer contained in the assay kit adding protease and phosphatase inhibitors mix. Next, a two-step assay procedure was used. The lysates (30 μL) were added to white 96-well half area plate. Mix of acceptor beads (15 μL) in the assay buffer was then added to the well. The plate was covered with a lid and incubated at room temperature for 1 h. Subsequently, 15 μL of donor beads in assay buffer were added, the plate was covered with a lid and incubated at room temperature for 1 h in the dark. The AlphaLISA signal was measured with EnSight™ Multimode Plate Reader (Perkin Elmer®). The Alpha signals of p-Akt were normalized to the Alpha signals of total Akt measured for all samples using AlphaScreen® SureFire HV™ Akt 1/2/3 total assay kit (Perkin Elmer).

RESULTS

Curcumin nanoparticles preparation and characterization. Although Cur holds great promise for application in cancer therapy and human health, it has been difficult to assess this molecule in its actual potential for several reasons. Among them, extremely poor water solubility (between 0.4 and 0.6 μg mL^{-1})[35,36] combined with fast degradation associated to low chemical stability under physiologic conditions strongly limit Cur pharmacological utility. In addition, the analytical assays designed to assess the biological effects of Cur are generally affected by the necessary solubilization with DMSO that could perturb the effect actually attributable to Cur. Hence, we reasoned that the incorporation of Cur inside the HFn shell could remarkably improve the chemical stability of the molecule and allow us to achieve aqueous solubility without the need of additional co-solvents. Thus, we first evaluated the ability of our nanoformulation to improve Cur stability in solution and to protect the incorporated drug from the external environment. The procedure we used for drug encapsulation into the HFn shell was based on the ability of HFn to modify its quaternary structure in response to pH changes. Unlike the conventional strategy adopted in most previous reports to encapsulate Cur, in which HFn was disassembled at acidic pH,[37,38] in the present work we preferred the alkaline disassembly of HFn. This allowed us to avoid the pre-solubilization of Cur in DMSO needed under acidic pH because Cur is instead soluble at high pH values. Unfortunately, Cur chemical stability is limited to around 2 h in 0.1 M aqueous sodium hydroxide, but increases at pH≥11.7.[39] For this reason, the reaction was run shortly (less than 30 min) at pH 12.5, then the pH was rapidly brought to neutrality allowing HFn to close the cage around Cur. The final product has been characterized with different techniques prior to the *in vitro* experiments.

Firstly, thanks to Raman spectroscopy we provided evidence about the encapsulation of Cur inside the HFn shell. As shown in Figure S3, Raman spectrum of Cur changed after incorporation into the HFn cavity. In particular, the band at 972 cm^{-1} relative to (C-OH) of enol group in the central portion of Cur drastically decreased in intensity. Besides, the intensity of the peak relative to the symmetric aromatic ring stretching at 1601 cm^{-1} was reduced while a new signal appeared at 1564 cm^{-1}.[40] No peak relative to HFn could be observed in the spectrum of CFn (Figure S3) due to a much lower cross-section of HFn in comparison to Cur. The fact that the bands most affected were those related to the aromatic ring and to the central enol group suggested that an interaction between HFn and Cur occurred and forced the drug to assume a different conformation. Commercially available Cur exists as enol tautomer where the two lateral aromatic rings have a twisted conformation.[41] Different planar polymorphs of Cur were reported in the literature, exhibiting the appealing characteristic of increasing the apparent water solubility. Raman spectra of these planar polymorphs were very similar to the one recovered in CFn spectra.[41] This observation allowed us to confirm that Cur was incorporated into the nanoparticle cavity in a conformation more readily dissolvable in water. Similar Raman spectra of Cur reported for an inclusion of the drug in cyclodextrines corroborated our observation.[42] UV-vis analysis of Cur content in HFn, conducted by incubating Cur and HFn at neutral pH,[37] confirmed that over 95% Cur was hosted inside the cavity (Table S1). In addition, we found that the protein yield was over 60% using our strategy (Table S2).

The improvement of Cur solubility resulting from its nanoformulation was confirmed by UV-vis measurements of CFn. Stable solutions at 374.1 ± 24.0 μg mL^{-1} final concentration of Cur could be easily obtained, which represents a 700-fold increase in solubility compared to the drug alone. This means that our method allowed us to accommodate 90 ± 7 Cur molecules in each

ferritin shell. The complex was stable for several days without losing Cur molecules, as demonstrated by the stability experiments described before.

As a result of the protection from the external environment, the molecular structure of Cur inside the cavity of HFn was long term stable, as confirmed again by UV-vis and Raman spectrophotometry analyses. Since Cur possess a typical absorption profile, a series of UV analyses were performed at both alkaline and physiologic conditions in order to confirm the stability increase of Cur in CFn compared to Cur alone. Free Cur exhibited a maximal absorption λ_{max} at ~430 nm, while Cur in CFn sample had λ_{max} at ~400 nm as a result of the structural changes mentioned above, suggesting a possible contribution of the protein complexation to the λ_{max} blue-shift. According to previous studies,[38,43] Cur decomposes rapidly at neutral pH as evidenced by the decrease over time of the peak intensity at 430 nm, whereas a new peak around 270 nm appeared probably due to degradation products (Figure 1A). In contrast, the characteristic peak of Cur incorporated inside HFn was only faintly affected after 48 h (Figure 1B), suggesting that encapsulated Cur retained the molecular stability, maintaining at least 70% integrity over time (Figure 1C). Stability analysis performed at pH 12.5 confirmed the rapid degradation of both Cur and CFn. Indeed, under these conditions, the protein shell opened and HFn was no longer able to protect Cur from degradation. As expected, the two profiles were similar (Figure S4). Raman spectroscopy also confirmed that Cur remained inside the nanoparticles maintaining the planar conformation for at least 72 h without any sign of recrystallization in the twisted configuration (Figure S5).

Figure 1. A) UV-vis spectra of Cur and B) CFn samples. C) Stability of free and encapsulated Cur, in PBS pH 7.2 at 25 °C, obtained by analyzing the absorption intensity of Cur (λ = 434 nm, green line) and CFn (λ = 403 nm, blue line).

Finally, we assessed the morphodimensional features of CFn by transmission electron microscopy (TEM) and dynamic light scattering (DLS) analyses. Figure 2A,B showed that CFn were spherical in shape with a size of about 12 nm, consistent with the structural conservation of the protein shell after Cur incorporation. This data is also supported by DLS, which provided a hydrodynamic size of 14.3 ± 4.3 nm (Figure 2C).

Next, we examined the behavior of Cur in organic and aqueous solution by DLS. Surprisingly, Cur, dissolved in DMSO and then diluted in PBS, appeared to generate a homogeneous particulate having a large hydrodynamic size (~1000 nm) attributable to a low aqueous solubility of Cur, whereas the DMSO solution of Cur provided a signal around 1 nm (Figure 2C).

Figure 2. A) Transmission electron micrograph of a layer of CFn resting on Formvar carbon film on copper grid. Scale bar = 50 nm. B) TEM size distribution. C) DLS analysis of 50 μM CFn diluted in PBS (blue line), compared to 50 μM Cur diluted in PBS (red line) or in DMSO (green line).

Interaction of CFn with TNBC cells. The recognition affinity of CFn for CTNBC and BTNBC and the capability to be internalized was assessed by flow cytometry (Figure 3).

Figure 3. Interaction of CFn with TNBC cells. For uptake analysis, MDA-MB-231 (A, C) and MDA-MB-468 cells (B, D) were treated with 50 μg mL^{-1} of CFn or HFn, both labeled with FITC, for 15 min, 1, 4, 24, 48 and 72 h at 37 °C. The mean fluorescence intensity was determined by flow cytometry.

We observed that CFn was taken up by both CTNBC and BTNBC cells with a maximum level of internalization at 24 h (Figure 3A,B). Interestingly, similar kinetics was observed for empty HFn (Figure 3C,D), suggesting that our preparation did not affect the functionality and targeting

efficiency of nanocages. To confirm that internalization was actually mediated by TfR1 through clathrin-dependent uptake,[30] all active endocytosis mechanisms were inhibited maintaining the cells at 4 °C for 2 h during the incubation with CFn-FITC. After the inhibition, we analyzed the binding of CFn-FITC with CTNBC and BTNBC cells by flow cytometry (Figure 4).

Figure 4. Effects of endocytosis inhibition on CFn internalization in BTNBC and CTNBC. Histograms represent the percentage of CFn-FITC (50 μg mL^{-1}) internalized by cells without endocytosis inhibition (grey histograms) and cells maintained at 4 °C for 2 h (blue histograms). The percentage of uptake was calculated by fluorescence intensity measured by flow cytometry setting at 100% cells without any inhibition. ***P<0.01 *vs.* CFn-FITC 37 °C after one-way ANOVA analysis.

Figure 4 confirmed that CFn exploited an active endocytosis pathway of entry because the CFn uptake was reduced of up to 77.0 ± 0.7% and 68.0 ± 0.7% in BTNBC and CTNBC cells, respectively, compared to physiologic condition at 37 °C. As reported by Illien *et al.*, the percentage obtained by this experiment represents also the estimation of CFn internalized by TNBC cells.[44] In fact, the signal at physiologic conditions was due both to CFn absorbed on the cell surfaces and to the one internalized by cells. The subtraction of 4 °C signals (only CFn absorbed on cell surfaces) provided the extent of actually internalized CFn.

Thanks to the typical vibrational signatures of CFn and Cur described above, the internalization of CFn in cells could be examined in depth by label-free confocal Raman imaging (Figure 5). The Raman spectra of CFn acquired as a reference have been fitted on all the imaging datasets showing that both BTNBC and CTNBC cells progressively internalized CFn along the first 24 h, but with different timing and mode. Raman false-color images of BTNBC cells

showed that after 15 min some CFn were observed in correspondence of the cellular margins. Between 4 and 24 h, CFn were abundantly taken up and observed in different regions of the cytoplasm. However, in CTNBC, CFn-related Raman signals were observed only after 4 h, mostly in proximity of the cellular membrane, and after 24 h in the cytoplasm, even if in a moderate extent compared to BTNBC. By observing the false color Raman images of both types of cells, it was also possible to appreciate the overlapping (merge, yellow channel) between CFn-related Raman signals (red channel) and some strong and clustered lipid/proteins signals in the cytoplasm, most probably related to endosomal/lysosomal vesicles, corroborating our hypothesis that a receptor-mediated endocytosis pathway should occur for CFn internalization, as anticipated by flow cytometry. This hypothesis was also confirmed by the colocalization of CFn-related Raman signals and some vesicles/vacuoles observable in bright field images. In general, the Raman features of the spectra acquired during in-cells imaging confirmed that Cur was mostly confined in the encapsulated form (CFn), at least at the beginning of the treatment. This is supported by the positive ratio between bands around 1634 and 1601 cm^{-1} and by the absence of the band around 961 cm^{-1} in the spectra recorded in cells (see reference spectra in Figure S3). At the same time, some spectral features changed significantly with incubation time. For example, the ratio between bands around 1634 and 1601 cm^{-1} drastically decreased, thus resembling the spectrum of free Cur, whereas the band around 1472 cm^{-1} progressively increased along the incubation. It is worth noting that the band around 1472 cm^{-1} was neither observed in Cur nor in CFn used both as reference substances or in cells. This particular band could be associated with C=N stretching,[45] however it was difficult to attribute the full molecular structures at this stage. Albeit out of the scope of the present study, disclosing the structural features of Cur metabolites emerged here will deserve further investigations in the future. Regardless of the nature of such

Cur derivative products, this effect suggested that CFn internalization could have triggered the activation of response mechanisms by the host cell, prompting us to investigate more thoroughly the possible involvement of different molecular pathways, related to defense, proliferation or cell death.

Figure 5. Confocal Raman imaging of CTNBC (A-L) and CTNBC (M-X) treated with CFn and measured at different incubation times. Bright field (left), false-color Raman images (middle) and classical least squares (CLS) fitting images (right) are reported. False-color Raman images were made by selecting and overlapping the intensities of the CH_2 bending mode of proteins and lipids (band between 1420-1470 cm^{-1}) (green) and of the two CFn bands in the range between 1600 and 1640 cm^{-1} (red). The CLS fitting images report the region with the highest fitting score (magenta) between the reference CFn spectra and the spectra acquired from the cells. For each experiment, a representative spectrum of the cytoplasm free from CFn (green), a representative spectrum of CFn localized inside the cells (red) was selected from the Raman images (arrows and arrowheads, respectively) and reported beside the images. In addition, the reference CFn spectra used for the CLS fitting was reported (magenta) for comparison. All the spectra were normalized and staked in the y-axis for clarity. In panel D, the Raman shifts of the bands discussed in the text are reported. Scale bars: 10 μm.

Comparison between Cur and CFn cytotoxicity in TNBC cells. The main aim of our work was to improve the anticancer activity of Cur against TNBC cells enhancing the solubility and the targeting efficiency of the molecule through the encapsulation in HFn nanocages. First, we determined the cytotoxicity of CFn compared to Cur in BTNBC and CTNBC cells by MTT viability assay treating both cell lines at increasing concentrations of drug in the range 5 to 50

μM and at different time points (Figure 6). This concentration range was established in accordance with previously reported data considering that the added volume of DMSO should not exceed 0.1% of the whole medium in each well.[24,46,47]

Figure 6. Cytotoxicity of Cur (A, B) and CFn (C, D) on TNBC cells. CTNBC (A, C) and BTNBC (B, D) cells were treated with different concentrations of Cur or CFn for 24, 48 and 72 h. Histograms represent the percentage of viable cells ± SD compared to control (untreated sample set at 100%). **P<0.05 *vs*. UNTR; ***P<0.01 *vs*. UNTR after one-way ANOVA analysis.

Figure 6 suggests that treatment with CFn is able to decrease the viability of both cell lines after 24 h also at 5 μM, which was not observed with Cur. This effect is more pronounced in BTNBC cells (Figure 6D), while in CTNBC cells (Figure 6C) the treatment progressively reached a plateau losing dose-dependence. The lower efficacy of CFn in CTNBC cells could be attributed to an impaired accumulation of Cur inside the cells, as already evidenced by confocal Raman images (Figure 5). However, we could assess that nanoformulation plays a pivotal role in enhancing the antitumor activity of the hydrophobic drug especially for BTNBC cells.

Cellular sensitization to cytotoxic treatment with doxorubicin. Cur has been shown to act as a chemosensitizer for different anticancer agents exploiting various mechanisms.[48] To assess if our nanoformulation could maintained or even increase this activity we decided to co-administer CFn with a chemotherapeutic drug typically subjected to chemoresistance, doxorubicin (Dox). We examined the cell viability at 24, 48 and 72 h incubating both TNBC cell lines with increasing Dox concentration (0.1 to 7.5 μM) together with three different

concentrations of CFn or free Cur (5, 10 and 20 μM Cur equivalents). MTT assay performed using BTNBC cells revealed that CFn increased the sensitization to Dox to a much higher extent than Cur alone already after 24 h even at the lowest concentration (Figure 7C, D). In CTNBC cells, we observed a slight increase of Dox cytotoxicity due to the presence of CFn only at 72 h treatment and, also in this case, 5 μM CFn was enough to get stronger effect compared to Cur. Differences between cell lines could be correlated to MTT data previously obtained (Figure 6), in which CFn had lower activity in CTNBC than in BTNBC cells.

Figure 7. Sensitization of breast cancer cells to doxorubicin mediated by Cur or CFn. Treatment of CTNBC and BTNBC cells with different concentrations of Dox (from 0.1 to 7.5 μM) with the addition of 5 and 20 μM Cur or CFn up to 72 h for CTNBC cells (A, B) and 24 h for BTNBC (C, D). *P<0.05 *vs.* Dox; ^P<0.05 *vs.* Dox + Cur after one-way ANOVA analysis. All other treatment combinations are shown in Figure S7.

One of the documented mechanisms by which Cur is able to sensitize tumor cells to chemotherapeutics takes advantage of the alteration of the functionality of multidrug resistance (MDR) transporter proteins (P-gp and MRP1) mediated by the inhibition of the protein efflux or by a decrease in the MDR gene expression.[46,49] Thus, we first assessed the presence of a basal MDR mechanism due to the presence of P-gp and MRP1 using a specific assay (eFluxx-ID Gold multidrug resistance assay kit). The assay is based on a hydrophobic non-fluorescent compound (EFLUXX-ID® dye) that penetrates the cell membrane to be subsequently hydrolyzed by the intracellular esterases that cleave the compound resulting in a fluorescence emission. In this way, the dye is entrapped inside the cells and can be effluxed out only by MDR proteins. The use of specific inhibitors of the MDR transporters, *i.e.*, verapamil for P-gp and MK571 for MRP1,

allowed us to determine the activity of a particular MDR protein by quantifying the variations in the residual dye signal by flow cytometry. Our analysis demonstrated that in both cell lines the activity of P-gp and MRP1 could be involved in drug resistance (Figure S6).

Once demonstrated the presence of MDR transporter proteins on both cell lines, we investigated the relationship between the effect observed in Figure 7 and the inhibition of the efflux pumps activity by Cur. In order to do this, we analyzed the efflux of Rhodamine 6G, a fluorescent dye used as a substrate of P-gp and MRP-1,[50] by TNBC cells. It is important to note that Cur has green fluorescence properties, which prompted us to use Rhodamine 6G for the experiments, having a non-interfering emission in the red wavelengths. The R6G fluorescence signal quantification in the supernatants was then correlated to the effluxing efficiency of MDR pump system. We observed that treatment with CFn reduced the efflux of R6G from both cell lines to a much higher extent compared to cells treated with Cur and to untreated cells (Figure 8). These data together with the MTT assay (Figure 7) confirmed that Cur could induce sensitization of TNBC cells through a mechanism presumably involving the efflux of Dox through MRP1 and P-gp.[46,49,51] Further investigations will be necessary to disclose the possible correlation of this result with a decrease in MDR protein expression.

Figure 8. Inhibition of Rhodamine 6G efflux by TNBC cells. After treating BTNBC (A) and CNTBC cells (B) with 1 μg mL^{-1} R6G for 1 h at 37 °C, 20 μM Cur or CFn were added and the fluorescence intensity of R6G was read in the supernatants at different time points. Data represent mean of three replicates ± SD.

Impact of CFn on cell cycle. Another important activity of Cur is the documented ability to modulate the cell cycle causing the accumulation of the cells in a G2/M or G0/G1 phase.[24,52,53]

By treating the two TNBC model cells with Cur for up to 48 h, we observed an accumulation in G2/M phase of BTNBC cells incubated with 20 μM Cur, confirming the data reported in our previous studies (Figure 9A).[24] However, the expected effect was not recovered in the case of CTNBC cells also at higher concentration of Cur (Figure 9B). On the other hand, nanoformulation of the molecule promoted the same G2/M block even at 5 μM of CFn in BTNBC cells, whereas CNTBC cells accumulated in G0/G1 phase (Figure 9C, D).

Once again, our results suggest that CFn nanoconstruct could enhance the activity of Cur, as occurred in the case of BTNBC cells, or reveal a new effect in CTNBC cells not detectable with Cur alone. Although unexpected, the observation of so different responses in the two TNBC models knowing was not surprising considering the molecular heterogeneity of these cognate tumors subtypes.[54] At the molecular level, Cur could target diverse signals capable of modulating the cell cycle and proliferation;[52] in particular, we focused here on an upstream key point associated to the PI3K/Akt pathway.

Figure 9. Cell cycle analysis of CTNBC and BTNBC cells treated with 5, 10 and 20 μM Cur and CFn up to 48 h. Cells were labeled with PI to determine the DNA content in each cell cycle phase by flow cytometry. Data represent the mean of percentage of cell distribution in each phase ± SD. **P<0.01 *vs*. UNTR after one-way ANOVA analysis.

Modulation of Akt phosphorylation. To evaluate the implication of PI3K/Akt pathway, we analyzed the levels of phosphorylated Akt (p-AKT) after treatment with Cur or CFn in both cell lines making use of Alpha Technology. Exploiting the high specificity of this bead-based proximity assay it is possible to quantify the amount of protein of interest in a faster way compared to Western blot. Figure 10A shows how the treatment with both Cur and CFn resulted,

in the case of BTNBC cells, in partial increased levels of p-AKT at early stages and a significant decrease after 24 h. In CTNBC no substantial alterations were revealed (Figure 10B). These results could corroborate the evidence from cell cycle and proliferation experiments. Indeed, the decrease of phosphorylation at Ser_{473} could lead to a downregulation of the Akt phosphorylation activity toward different proteins involved in cell cycle progression and proliferation, including $p27^{kip1}$ and mTOR, as widely documented in several reports.[55-57]

Figure 10. Analysis of p-Akt (Ser_{473}) with Alpha technology. BTNBC (A) and CTNBC (B) cells were treated with 20 μM Cur or CFn for 1, 4 and 24 h. Alpha signals were read with Ensight multiplate reader (Perkin Elmer), normalized on Akt total signals and represented as mean ± SD. **P<0.05 *vs.* UNTR; ***P<0.01 *vs.* UNTR after one-way ANOVA analysis.

DISCUSSION

Turmeric offers a great potential as a source of a natural therapeutic such as curcumin, recognized as safe. Unfortunately, curcumin does not possess the characteristics that would make it a good drug candidate, and even though it is known since centuries and multiple therapeutic activities are ascribed to it, it still has dark sides, enough to be considered an "invalid metabolic panaceas".[16]

In this work, we took advantage of H-Ferritin (HFn) to develop a biomimetic nanosystem that allowed us to overcome some of the most critical issues related to curcumin utilization, including poor solubility, chemical instability, and low bioavailability. In addition, HFn maintains the capability of self-assembling, disassembling and reassembling with shape memory into a 24-H subunit nanocage depending on pH changes. Apoferritin was recently explored as a strategy to improve the water solubility of curcumin obtaining stable nanoparticles with narrow size

distribution. Besides H-Ferritin nanocages,[58] also L-Ferritin or horse spleen apoferritin (containing 85% L and 15% H chains) were used to encapsulate curcumin with good results.[59,60] In some cases, theranostic nanosystems were obtained combining incorporation of curcumin and magnetic resonance imaging contrast agents, such as Gd(III) and Mn(II) ions.[60] In all of these works, a loading procedure under acidic conditions was followed.

With our method exploiting basic pH, Cur could be loaded in a straightforward and reproducible manner obtaining loading yields much higher than previous reports using H-Ferritin, in which the incorporation was accomplished under conventional acidic conditions.[58] Noteworthy, we worked with pure Cur, purified from a commercial mixture by flash chromatography on silica gel. In this way, we focused on a single active molecule, removing possible ambiguities that are often associated with the use of curcumin or, more in general, of turmeric extracts.

The characterization of CFn let us appreciate that encapsulated Cur presented a characteristic structure inside the HFn cavity, was stable over time and significantly more soluble and available than the free molecule. At the same time, HFn maintained its morphological feature and its ability to be recognized and actively internalized by two different kinds of triple negative breast cancer cell models, MDA-MB-231 and MDA-MB-468, representative of the claudin-low and basal TNBC subtypes, respectively. The internalization of CFn by TNBC cells was demonstrated by flow cytometry using FITC labeled CFn. In addition, label-free confocal Raman imaging was used to confirm and study the localization of unlabeled CFn at subcellular level, at different incubation times.

We compared the effect of our curcumin nanoformulation (CFn) with that of free curcumin, by assaying their effect on triple negative breast cancer cell lines, which are refractory to the

treatment with common cytotoxic drugs and lack specific receptors that could allow for a targeted therapy. As expected, binding experiments confirmed that HFn cages were internalized rapidly by both TNBC cell lines and this process was indeed mediated by the TfR1, resulting in a clathrin-dependent uptake.[28,61,62] The results obtained from viability assays revealed that CFn at minimal concentration was more effective compared to the drug alone. This was probably due to various factors, including the increase in solubility and chemical stability, but also because Cur, within this concentration range, exhibited a tendency to form colloidal aggregates, as suggested by DLS, which strongly affected the biological activity making the effect unpredictable.

In the attempt to elucidate the mechanisms behind the impact of nanoformulation, we investigated two well-known anticancer activities of Cur, including the chemosensitization and the alteration of cell cycle. MDR protein activity analysis combined with an efflux assay provided evidence that CFn preserved Cur feature to chemosensitize cells to the action of chemotherapeutics (*e.g.*, Dox), enhancing the cytotoxic effect of Dox by compromising the ATP-binding cassette transporter protein activity. In addition, CFn exhibited different cell cycle effects on these two TNBC cell lines. Indeed, MDA-MB-231 were blocked in G0/G1 phase whereas MDA-MB-468 accumulated in G2/M phase after 48 h of treatment. These results suggest that the impact of CFn on the cell cycle is strictly dependent on intrinsic cell features.

It is generally accepted that Cur has a pleiotropic effect, as it can interfere with several molecular targets simultaneously acting on multiple cellular pathways.[63] We therefore analyzed the PI3K/Akt pathway as a key point involved in many regulation mechanisms of tumor cells. AlphaLISA Technology demonstrated that CFn was able to induce a decrease in the extent of Akt phosphorylation as Cur alone did, suggesting that the signal cascade regulated by PI3K/Akt would be altered, thus impacting the proliferation and cell cycle.

Despite curcumin has attracted increasing interest in the scientific community, the actual potential of this molecule toward an effective utilization in the clinical practice has been recently questioned. Our results suggest that the design of Cur nanoparticles synthesized by alkaline incorporporation inside a HFn biopolymeric nanocage might provide us with soluble Cur endowed with high targeting efficiency toward cancer cells. The good experimental reliability allowed by HFn formulation of Cur holds great promise for the implementation of curcumin in the clinical investigation and may contribute to a reappraisal of this nutraceutical in medicine.

ASSOCIATED CONTENT

Supporting Information. This material (PDF file) is available free of charge via the Internet at http://pubs.acs.org.
Figure S1. Curcumin purification evaluated with thin-layer chromathography.
Figure S2. Curcumin calibration curve in acetic acid.
Figure S3. Raman spectra of HFn, Cur and CFn.
Figure S4. Stability of free and encapsulated curcumin in alkaline environment.
Figure S5. Stability by Raman spectroscopy.
Figure S6. Native PAGE of HFn and CFn.
Figure S7. Basal expression of MDR transporters.
Figure S8. Cytotoxicity of free curcumin and CFn in combination with doxorubicin.
Table S1. Nonspecific interaction of curcumin with HFn.
Table S2. Protein yield after curcumin encapsulation.

AUTHOR INFORMATION

Corresponding Author

* Prof. Dr. Davide Prosperi. Phone (+39) 02 6448 3302. Email: davide.prosperi@unimib.it.

Website: http://www.nanobiolab.btbs.unimib.it

Author Contributions

The manuscript was written through contributions of all authors. All authors have given approval to the final version of the manuscript. ‡These authors contributed equally.

ACKNOWLEDGMENT

This work was partly supported by the Fondazione Regionale per la Ricerca Biomedica (FRRB, grant 2015), Fondazione Cariplo-Regione Lombardia (Grant 2016-0886), and Academic Funding Unimib 2016.

REFERENCES

(1) Badve, S.; Dabbs, D. J.; Schnitt S. J.; Baehner, F. L.; Decker, T.; Eusebi, V.; Fox, S. B.; Ichihara, S.; Jacquemier, J.; Lakhani, S. R.; Palacios, J.; Rakha1, E. A.; Richardson, A. L.; Schmitt, F. C.; Tan, P. H.; Tse, G. M.; Weigelt, B.; Ellis, I. O.; Reis-Filho, J. S. Basal-like and triple-negative breast cancers: a critical review with an emphasis on the implications for pathologists and oncologists. *Mod. Pathol.* **2011,** *24*, 157–167.

(2) Foulkes, W. D.; Smith, I. E.; Reis-Filho J. S. Triple negative breast cancers. *N. Engl. J. Med*. **2010**, *363*, 1938–1948.

(3) Perou, C. M.; Sørlie, T.; Eisen, M. B.; van de Rijn, M.; Jeffrey, S. S.; Rees, C. A.; Pollack, J. R.; Ross, D. T.; Johnsen, H.; Akslen, L. A.; Fluge, O.; Pergamenschikov, A.; Williams, C.; Zhu, S. X.; Lønning, P. E.; Børresen-Dale, A. L.; Brown, P. O.; Botstein, D. Molecular portraits of human breast tumours. *Nature*. **2000**, *406*, 747–752.

(4) Sørlie, T.; Perou, C. M.; Tibshirani, R.; Aas, T.; Geisler, S.; Johnsen, H.; Hastie, T.; Eisen, M. B.; van de Rijn, M.; Jeffrey, S. S.; Thorsen, T.; Quist, H.; Matese, J. C.; Brown, P. O.; Botstein, D.; Lønning, P. E.; Børresen-Dale, A. L. Gene expression patterns of breast carcinomas distinguish tumor subclasses with clinical implications. *Proc. Natl. Acad. Sci. U. S. A.* **2001**, *98*, 10869–10874.

(5) Holliday, D. L.; Speirs, V. Choosing the right cell line for breast cancer research. *Breast Cancer Res*. **2011**, *13*, 215.

(6) André, F.; Zielinski, C. C. Optimal strategies for the treatment of metastatic triple-negative breast cancer with currently approved agents. *Ann. Oncol.* **2012**, *23*, vi46–vi51.

(7) Palmieri, C.; Krell, J.; James, C. R.; Harper-Wynne, C.; Misra, V.; Cleator, S.; Miles D. Rechallenging with anthracyclines and taxanes in metastatic breast cancer. *Nat. Rev. Clin. Oncol.* **2010**, *7*, 561–574.

(8) Burstein, H. J.; Elias, A. D.; Rugo, H. S.; Cobleigh, M. A.; Wolff, A. C.; Eisenberg, P. D.; Lehman, M.; Adams, B. J.; Bello, C. L.; De Primo, S. E.; Baum, C. M.; Miller, K. D. Phase II study of sunitinib malate, an oral multitargeted tyrosine kinase inhibitor, in patients with metastatic breast cancer previously treated with an anthracycline and a taxane. *J. Clin. Oncol.* **2008**, *26*, 1810–1816.

(9) Corkery, B.; Crown, J.; Clynes, M.; O'Donovan, N. Epidermal growth factor receptor as a potential therapeutic target in triple-negative breast cancer. *Ann. Oncol*. **2009**, *20*, 862–867.

(10) O'Reilly, E. A.; Gubbins, L.; Sharma, S.; Tully, R.; Guang, M. H.; Weiner-Gorzel, K.; McCaffrey, J.; Harrison, M.; Furlong, F.; Kell, M.; McCann, A. The fate of chemoresistance in triple negative breast cancer (TNBC). *BBA Clin*. **2015**, *3*, 257–275.

(11) Shishodia, S.; Sethi, G.; Aggarwal B. B. Curcumin: getting back to the roots. *Ann. N.Y. Acad. Sci.* **2005**, *1056*, 206–217.

(12) Esatbeyoglu, T.; Huebbe, P.; Ernst, I. M.; Chin, D.; Wagner, A. E.; Rimbach, G. Curcumin - From molecule to biological function. *Angew. Chem. Int. Ed. Engl.* **2012**, *51*, 5308–5332.

(13) Mahmood, K.; Zia, K. M.; Zuber, M.; Salman, M.; Anjum, M. N. Recent Developments in Curcumin and Curcumin Based Polymeric Materials for Biomedical Applications: a Review. *Int. J. Biol. Macromol*. **2015**, *81*, 877–890.

(14) Aggarwal, B. B.; Kumar, A.; Bharti A. C. Anticancer Potential of Curcumin: Preclinical and Clinical Studies. *Anticancer Res.* **2003**, *23*, 363–398.

(15) Kunnumakkara, A. B.; Bordoloi, D.; Padmavathi, G.; Monisha, J.; Roy, N. K.; Prasad, S.; Aggarwal, B. B. Curcumin, the Golden Nutraceutical: Multitargeting for Multiple Chronic Diseases. *Br. J. Pharmacol*. **2016**, *174*, 1325–1348.

(16) Nelson, K. M.; Dahlin, J. L.; Bisson, J.; Graham, J.; Pauli, G. F.; Walters, M. A. The Essential Medicinal Chemistry of Curcumin. *J. Med. Chem.* **2017**, *60*, 1620–1637.

(17) Yang, K. Y.; Lin, L. C.; Tseng, T. Y.; Wang, S. C.; Tsai, T. H. Oral Bioavailability of Curcumin in Rat and the Herbal Analysis from *Curcuma longa* by LC–MS/MS. *J. Cromatogr. B: Anal. Technol. Biomed. Life Sci*. **2007**, *853*, 183–189.

(18) Sharma, R. A.; McLelland, H. R.; Hill, K. A.; Ireson, C. R.; Euden, S. A.; Manson, M. M.; Pirmohamed, M.; Marnett, L. J.; Gescher, A. J.; Steward, W. P. Pharmacodynamic and Pharmacokinetic Study of Oral *Curcuma* Extract in Patients with Colorectal Cancer. *Clin. Cancer Res*. **2001**, *7*, 1894–1900.

(19) Shoba, G.; Joy, D.; Joseph, T.; Majeed, M.; Rajendran, R.; Srinivas, P. S. Influence of Piperine on the Pharmacokinetics of Curcumin in Animals and Human Volunteers. *Planta Med*. **1998**, *64*, 353–356.

(20) Anand, P.; Kunnumakkara, A. B.; Newman, R. A.; Aggarwal, B. B. Bioavailability of Curcumin: Problems and Promises. *Mol. Pharmaceutics*. **2007**, *4*, 807–818.

(21) Vyas, A.; Dandawate, P.; Padhye, S.; Ahmad, A.; Sarkar, F. Perspectives on New Synthetic Curcumin Analogs and their Potential Anticancer Properties. *Curr. Pharm. Des.* **2013**, *19*, 2047–2069.

(22) Ghalandarlaki, N.; Alizadeh, A. M.; Ashkani-Esfahani, S. Nanotechnology-Applied Curcumin for Different Diseases Therapy. *BioMed Res. Int*. **2014**, *2014*, 394264.

(23) Wang, J.; Wang, Y.; Liu, Q.; Yang, L.; Zhu, R.; Yu, C.; Wang, S. Rational Design of Multifunctional Dendritic Mesoporous Silica Nanoparticles to Load Curcumin and Enhance Efficacy for Breast Cancer Therapy. *ACS Appl. Mater. Interfaces*. **2016**, *8*, 26511–26523.

(24) Verderio, P.; Bonetti, P.; Colombo, M.; Pandolfi, L.; Prosperi, D. Intracellular Drug Release from Curcumin-Loaded PLGA Nanoparticles Induces G2/M Block in Breast Cancer Cells. *Biomacromolecules*. **2013**, *14*, 672–682.

(25) Avvakumova, S.; Colombo, M.; Tortora, P.; Prosperi D. Biotechnological approaches toward nanoparticle biofunctionalization. *Trends in Biotechnol.* **2014**, *32*, 11–20.

(26) Arosio, P.; Ingrassia, R.; Cavadini, P. Ferritins: a family of molecules for iron storage, antioxidation and more. *Biochim. Biophys. Acta*. **2009**, *1790*, 589–99.

(27) Crichton, R. R.; Bryce, C. F. Subunit interactions in horse spleen apoferritin. Dissociation by extremes of pH. *Biochem. J.* **1973**, *133*, 289–299.

(28) Bellini, M.; Mazzucchelli, S.; Galbiati, E.; Sommaruga, S.; Fiandra, L.; Truffi, M.; Rizzuto, M. A.; Colombo, M.; Tortora, P.; Corsi, F.; Prosperi, D. Protein nanocages for self-triggered nuclear delivery of DNA-targeted chemotherapeutics in Cancer Cells. *J. Controlled Rel*. **2014**, *196*, 184–196.

(29) Maham, A.; Tang, Z.; Wu, H.; Wang, J.; Lin, Y. Protein-Based Nanomedicine Platform for Drug Delivery. *Small*. **2009**, *5*, 1706–1721.

(30) Li, L.; Fang, C. J.; Ryan, J. C.; Niemi, E. C.; Lebrón, J. A.; Björkman, P. J.; Arase, H.; Torti, F. M.; Torti, S. V.; Nakamura, M. C.; Seaman, W. Binding and uptake of H-ferritin are mediated by human transferrin receptor-1. *Proc. Natl. Acad. Sci. U. S. A.* **2010**, *107*, 3505–3510.

(31) Fan, K.; Cao, C.; Pan, Y.; Lu, D.; Yang, D.; Feng, J.; Song, L.; Liang, M.; Yan, X. Magnetoferritin nanoparticles for targeting and visualizing tumour tissues. *Nat Nanotechnol*. **2012,** *7*, 459–464.

(32) Daniels, T. R.; Bernabeu, E.; Rodríguez, J. A.; Patel, S.; Kozman, M.; Chiappetta, D. A.; Holler, E.; Ljubimova, J. Y.; Helguera, G.; Penichet, M. L. The Transferrin Receptor and the Targeted Delivery of Therapeutic Agents Against Cancer. *Biochim. Biophys. Acta*. **2012**, *1820*, 291–317.

(33) Péret-Almeida, L.; Cherubino, A. P. F.; Alves, R. J.; Dufossé, L.; Glória, M. B. A. Separation and determination of the physico-chemical characteristics of curcumin, demethoxycurcumin and bisdemethoxycurcumin. *Food Res. Int.* **2005**, *38*, 1039–1044.

(34) Masuda, T.; Goto, F.; Yoshihara, T.; Mikami, B. The Universal Mechanism for Iron Translocation to the Ferroxidase Site in Ferritin, which is Mediated by the Well Conserved Transit Site. *Biochem. Biophys. Res. Commun*. **2010,** *400*, 94–99.

(35) Yallapu, M. M.; Jaggi, M.; Chauhan, S. C. Curcumin nanoformulations: a future nanomedicine for cancer. *Drug Discovery Today* **2012,** *17*, 71–80.

(36) Naksuriya, O.; Okonogi, S.; Schiffelers, R. M.; Hennink, W. E. Curcumin nanoformulations: a review of pharmaceutical properties and preclinical studies and clinical data related to cancer treatment. *Biomaterials*, **2014**, *35*, 3365–3383.

(37) Cutrin J. C.; Crich, S. G.; Burghelea, D.; Dastrù, W.; Aime S. Curcumin/Gd loaded apoferritin: a novel "theranostic" agent to prevent hepatocellular damage in toxic induced acute hepatitis. *Mol. Pharmaceutics.* **2013,** *10*, 2079–2085.

(38) Chen, L.; Bai, G.; Yang, S.; Yang, R.; Zhao, G.; Xu, C.; Leung, W. Encapsulation of curcumin in recombinant human H-chain ferritin increases its water-solubility and stability, *Food Res. Int.* **2014**, *62*, 1147–1153.

(39) Bernabé-Pineda, M.; Ramírez-Silva, M. T.; Romero-Romo, M.; González-Vergara, E.; Rojas-Hernández, A. Determination of acidity constants of curcumin in aqueous solution and apparent rate constant of its decomposition. *Spectrochim. Acta. A. Mol. Biomol. Spectrosc.* **2004**, *60*, 1091–1097.

(40) López-Tobar, E.; Blanch, G. P.; Ruiz del Castillo, M. L.; Sánchez-Cortés, S. Encapsulation and isomerization of curcumin with cyclodextrins characterized by electronic and vibrational spectroscopy. *Vib. Spectrosc*. **2012**, *62*, 292–298.

(41) Sanphui, P.; Goud, N. R.; Khandavilli, U. B.; Bhanoth, S.; Nangia, A. New polymorphs of curcumin. *Chem. Commun*. **2011**, *47*, 5013–5015.

(42) Mohan, P.R. K.; Sreelakshmi, G.; Muraleedharan, C. V.; Joseph, R. Water soluble complexes of curcumin with cyclodextrins: Characterization by FT-Raman spectroscopy. *Vib. Spectrosc*. **2012**, *62*, 77– 84.

(43) Wang, Y. J.; Pan, M. H.; Cheng, A. L.; Lin, L. I.; Ho, Y. S.; Hsieh, C. Y.; Lin, J. K. Stability of curcumin in buffer solutions and characterization of its degradation products. *J. Pharm. Biomed. Anal.* **1997**, *15*, 1867–1876

(44) Illien, F.; Rodriguez, N.; Amoura, M.; Joliot, A.; Pallerla, M.; Cribier, S.; Burlina, F.; Sagan, S. Quantitative fluorescence spectroscopy and flow cytometry analyses of cell-penetrating peptides internalization pathways: optimization, pitfalls, comparison with mass spectrometry quantification. *Sci. Rep*. **2016**, 6, 36938.

(45) Naumann, D. Infrared and NIR Raman spectroscopy in medical microbiology. *Proc. SPIE*. **1998***, 3257*, 245–257.

(46) Anuchapreeda, S.; Leechanachai, P.; Smith, M. M.; Ambudkar, S. V.; Limtrakul, P. N. Modulation of P-glycoprotein expression and function by curcumin in multidrug-resistant human KB cells. *Biochem. Pharmacol*. **2002**, *64*, 573–582.

(47) Cridge, B. J.; Larsen, L.; Rosengren, R. J. Curcumin and its derivatives in breast cancer: Current developments and potential for the treatment of drug-resistant cancers. *Oncology Discovery*. **2013**, DOI: 10.7243/2052-6199-1-6.

(48) Goel, A.; Aggarwal, B. B. Curcumin, the golden spice from Indian saffron, is a chemosensitizer and radiosensitizer for tumors and chemoprotector and radioprotector for normal organs. *Nutr. Cancer*. **2010**, *62*, 919–30.

(49) Limtrakul, P.; Chearwae, W.; Shukla, S.; Phisalphong, C.; Ambudkar, S. V. Modulation of function of three ABC drug transporters, P-glycoprotein (ABCB1), mitoxantrone resistance protein (ABCG2) and multidrug resistance protein 1 (ABCC1) by tetrahydrocurcumin, a major metabolite of curcumin. *Mol. Cell. Biochem.* **2007**, *296*, 85–95.

(50) Saengkhae, C.; Loetchutinat, C.; Garnier-Suillerot, A. Kinetic analysis of rhodamines efflux mediated by the multidrug resistance protein (MRP1). *Biophys J*. **2003**, *85*, 2006–2014.

(51) Ampasavate, C.; Sotanaphun, U, Phattanawasin P, Piyapolrungroj N. Effects of Curcuma spp. on P-glycoprotein function. *Phytomedicine*. **2010**, *17*, 506–512.

(52) Sa, G.; Das, T. Anti cancer effects of curcumin: cycle of life and death. *Cell Div*. **2008**, *3*, 14.

(53) Choudhuri, T.; Pal, S.; Das, T.; Sa, G. Curcumin selectively induces apoptosis in deregulated cyclin D1-expressed cells at G2 phase of cell cycle in a p53-dependent manner. *J. Biol. Chem.* **2005**, *280*, 20059–20068.

(54) Irshad, S.; Ellis, P.; Tutt, A. Molecular heterogeneity of triple-negative breast cancer and its clinical implications. *Curr. Opin. Oncol*. **2011**, *23*, 566–577.

(55) Fresno Vara, J. A.; Casado, E.; de Castro, J.; Cejas, P.; Belda-Iniesta, C.; González-Barón M. PI3K/Akt signalling pathway and cancer. *Cancer Treat. Rev.* **2004**, *30*, 193–204.

(56) LoPiccolo, J.; Blumenthal, G. M.; Bernstein, W. B.; Dennis, P.A. Targeting the PI3K/Akt/mTOR pathway: effective combinations and clinical considerations. *Drug Resist. Updates*. **2008**, *11*, 32–50.

(57) Hassan, B.; Akcakanat, A.; Holder, A. M.; Meric-Bernstam, F. Targeting the PI3-kinase/Akt/mTOR signaling pathway. *Surg. Oncol. Clin. N. Am*. **2013**, *22*, 641–664.

(58) Chen, L.; Bai, G.; Yang, S.; Yang, R.; Zhao, G.; Xu, C. Leung, W. Encapsulation of curcumin in recombinant human H-chain ferritin increases its water-solubility and stability. *Food Res. Int.* **2014**, *62*, 1147–1153.

(59) Conti, L.; Lanzardo, S.; Ruiu, R.; Cadenazzi, M.; Cavallo, F.; Aime, S.; Geninatti Crich, S. L-Ferritin targets breast cancer stem cells and delivers therapeutic and imaging agents. *Oncotarget* **2016**, *7*, 66713–66727.

(60) Geninatti Crich, S.; Cadenazzi, M.; Lanzardo, S.; Conti, L.; Ruiu, R.; Alberti, D.; Cavallo, F.; Cutrin, J. C.; Aime, S. Targeting ferritin receptors for the selective delivery of imaging and therapeutic agents to breast cancer cells. *Nanoscale* **2015**, *7*, 6527–6533.

(61) Mazzucchelli, S.; Bellini, M.; Fiandra, L.; Truffi, M.; Rizzuto, M. A.; Sorrentino, L.; Longhi, E.; Nebuloni, M.; Prosperi, D.; Corsi, F. Nanometronomic treatment of 4T1 breast cancer with nanocaged doxorubicin prevents drug resistance and circumvents cardiotoxicity. *Oncotarget*. **2017**, *8*, 8383–8396.

(62) Zhang, L.; Li, L.; Di Penta, A., Carmona, U., Yang, F.; Schöps, R.; Brandsch, M.; Zugaza, J. L.; Knez, M. H-Chain Ferritin: A Natural Nuclei Targeting and Bioactive Delivery Nanovector. *Adv. Healthc. Mater*. **2015**, 4, 1305–1310.

(63) Hatcher, H.; Planalp, R.; Cho, J.; Torti, F. M.; Torti, S. V. Curcumin: from ancient medicine to current clinical trials. *Cell. Mol. Life Sci*. **2008**, *65*, 1631–1652.

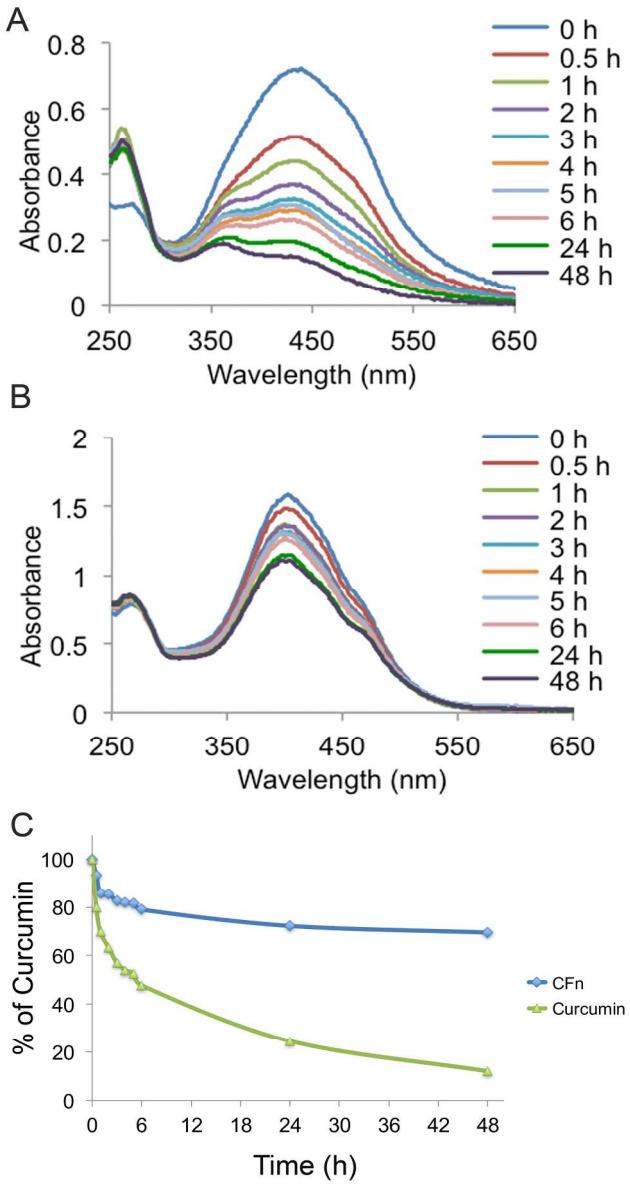

Figure 1. A) UV-vis spectra of Cur and B) CFn samples. C) Stability of free and encapsulated Cur, in PBS pH 7.2 at 25 °C, obtained by analyzing the absorption intensity of Cur (λ = 434 nm, green line) and CFn (λ = 403 nm, blue line).

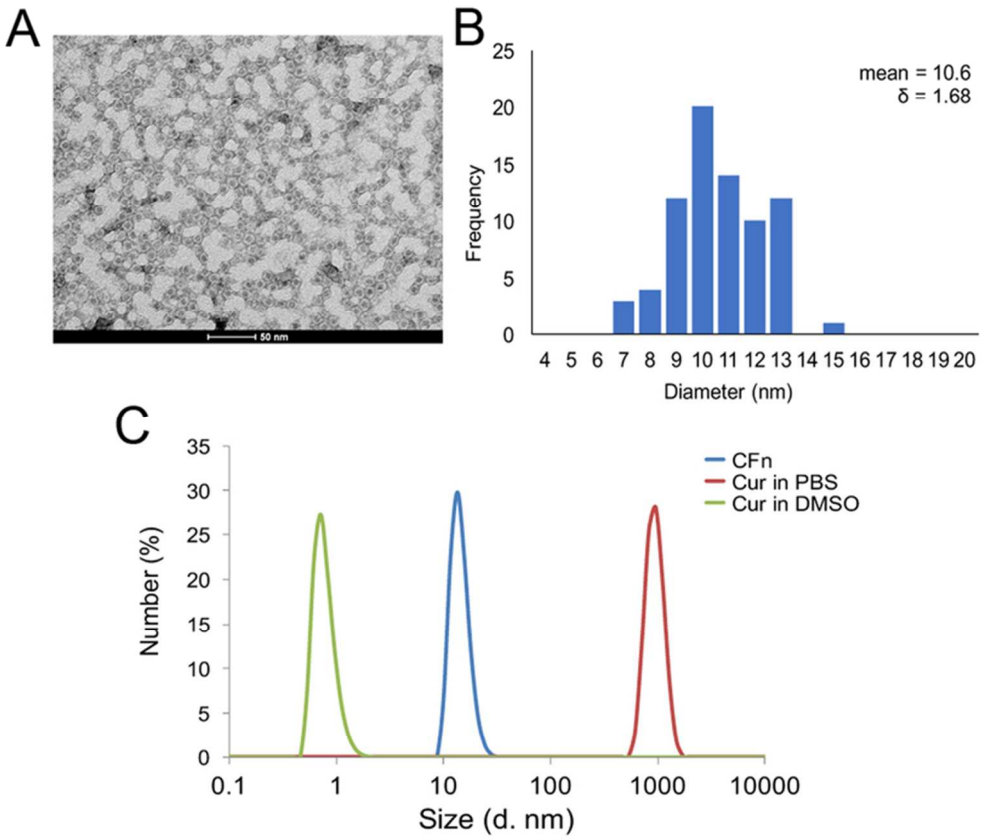

Figure 2. A) Transmission electron micrograph of a layer of CFn resting on Formvar carbon film on copper grid. Scale bar = 50 nm. B) TEM size distribution. C) DLS analysis of 50 μM CFn diluted in PBS (blue line), compared to 50 μM Cur diluted in PBS (red line) or in DMSO (green line).

69x59mm (300 x 300 DPI)

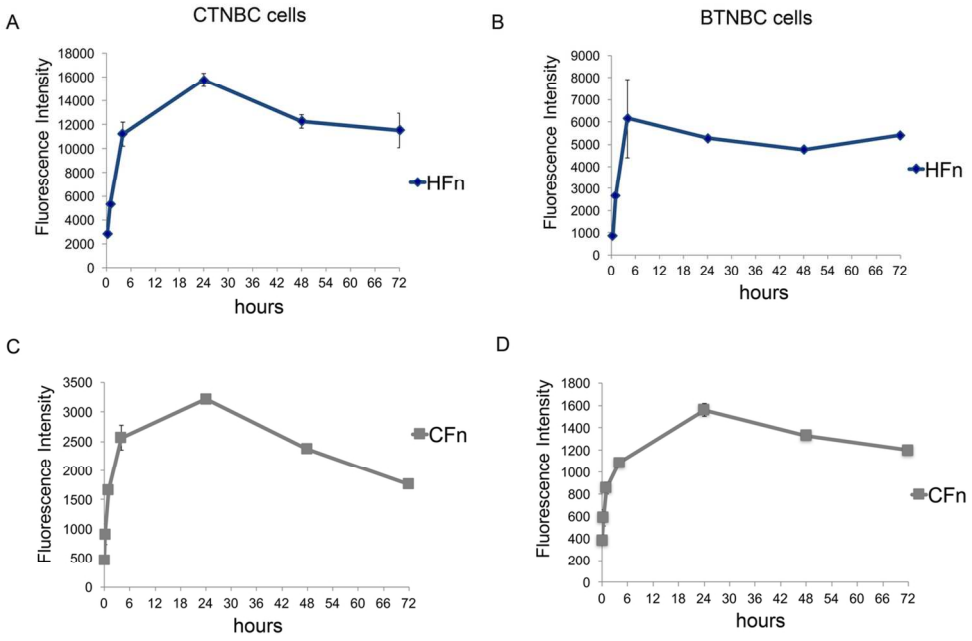

Figure 3. Interaction of CFn with TNBC cells. For uptake analysis, MDA-MB-231 (A, C) and MDA-MB-468 cells (B, D) were treated with 50 μg mL^{-1} of CFn or HFn, both labeled with FITC, for 15 min, 1, 4, 24, 48 and 72 h at 37 °C. The mean fluorescence intensity was determined by flow cytometry.

118x79mm (300 x 300 DPI)

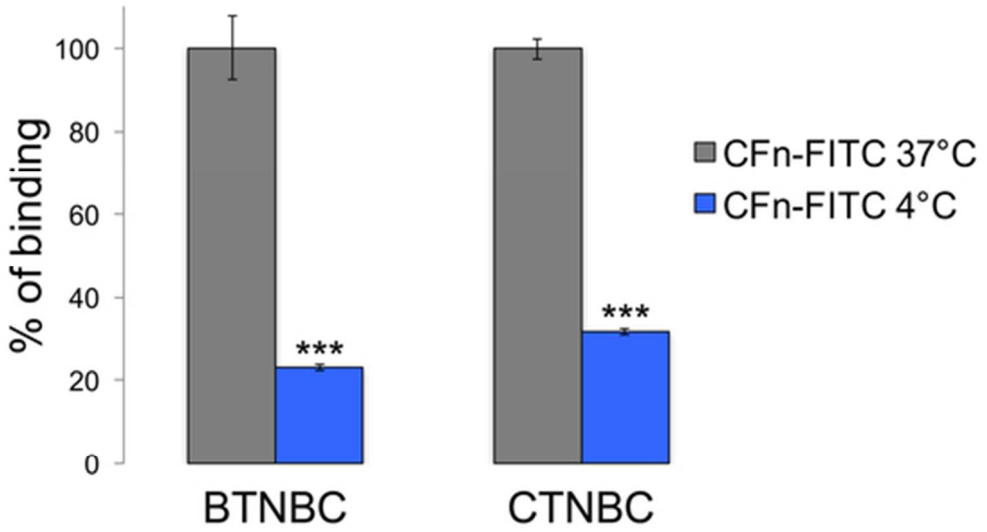

Figure 4. Effects of endocytosis inhibition on CFn internalization in BTNBC and CTNBC. Histograms represent the percentage of CFn-FITC (50 g mL^{-1}) internalized by cells without endocytosis inhibition (grey histograms) and cells maintained at 4 °C for 2 h (blue histograms). The percentage of uptake was calculated by fluorescence intensity measured by flow cytometry setting at 100% cells without any inhibition. ***P<0.01 vs. CFn-FITC 37 °C after one-way ANOVA analysis.

46x26mm (300 x 300 DPI)

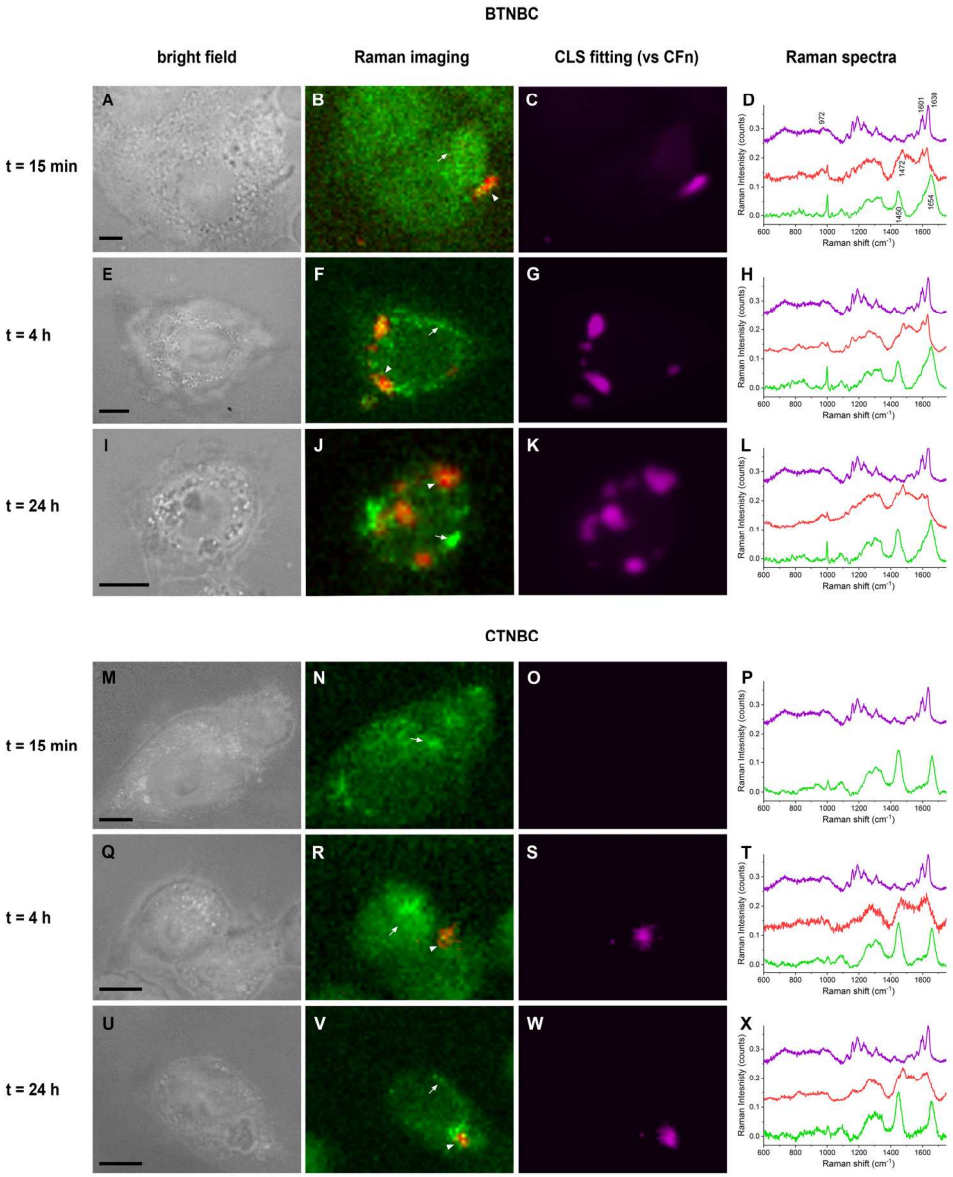

Figure 5. Confocal Raman imaging of CTNBC (A-L) and CTNBC (M-X) treated with CFn and measured at different incubation times. Bright field (left), false-color Raman images (middle) and classical least squares (CLS) fitting images (right) are reported. False-color Raman images were made by selecting and overlapping the intensities of the CH_2 bending mode of proteins and lipids (band between 1420-1470 cm^{-1}) (green) and of the two CFn bands in the range between 1600 and 1640 cm^{-1} (red). The CLS fitting images report the region with the highest fitting score (magenta) between the reference CFn spectra and the spectra acquired from the cells. For each experiment, a representative spectrum of the cytoplasm free from CFn (green), a representative spectrum of CFn localized inside the cells (red) was selected from the Raman images (arrows and arrowheads, respectively) and reported beside the images. In addition, the reference CFn spectra used for the CLS fitting was reported (magenta) for comparison. All the spectra were normalized and staked in the y-axis for clarity. In panel D, the Raman shifts of the bands discussed in the text are reported. Scale bars: 10 μμm.

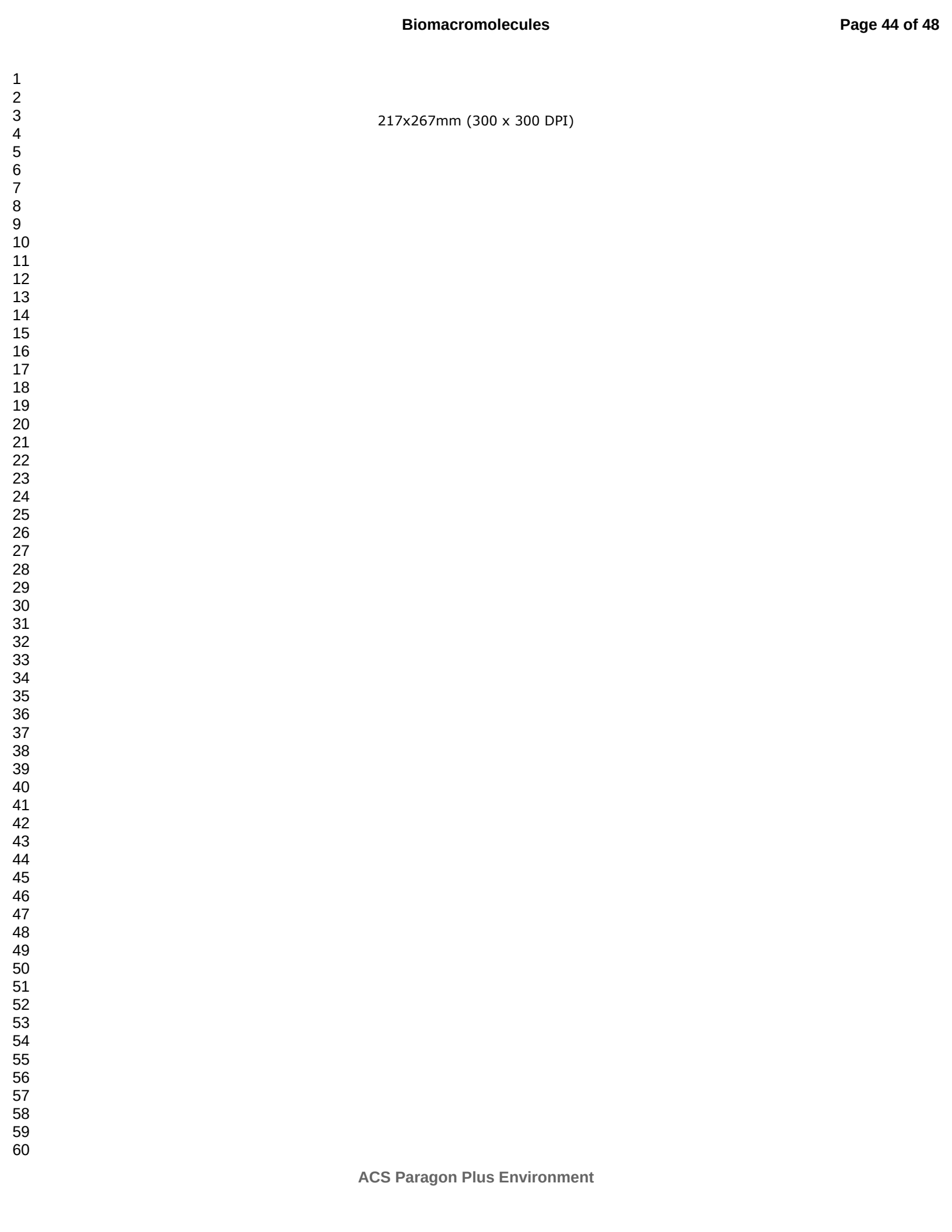
217x267mm (300 x 300 DPI)

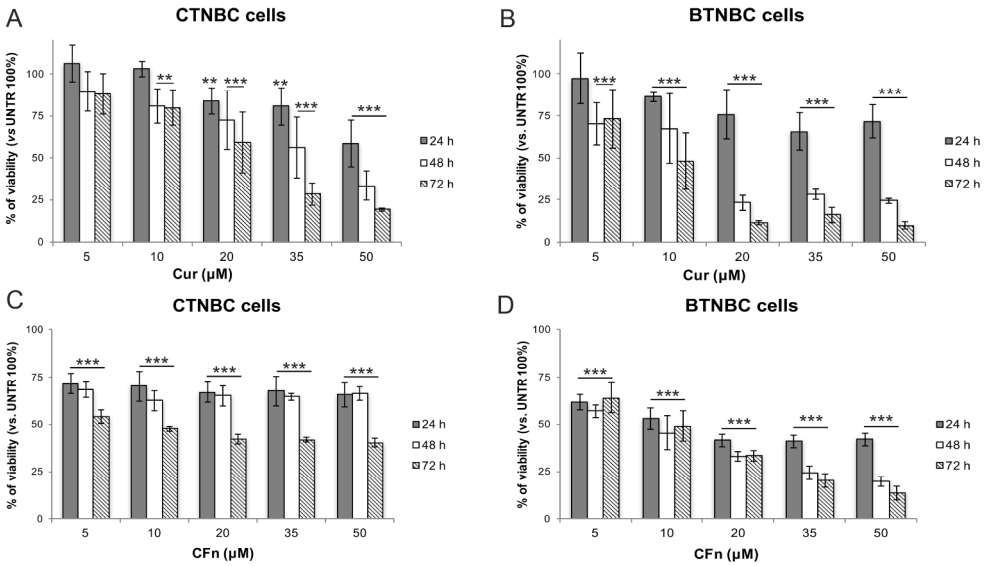

Figure 6. Cytotoxicity of Cur (A, B) and CFn (C, D) on TNBC cells. CTNBC (A, C) and BTNBC (B, D) cells were treated with different concentrations of Cur or CFn for 24, 48 and 72 h. Histograms represent the percentage of viable cells ± SD compared to control (untreated sample set at 100%). **P<0.05 vs. UNTR; ***P<0.01 vs. UNTR after one-way ANOVA analysis.

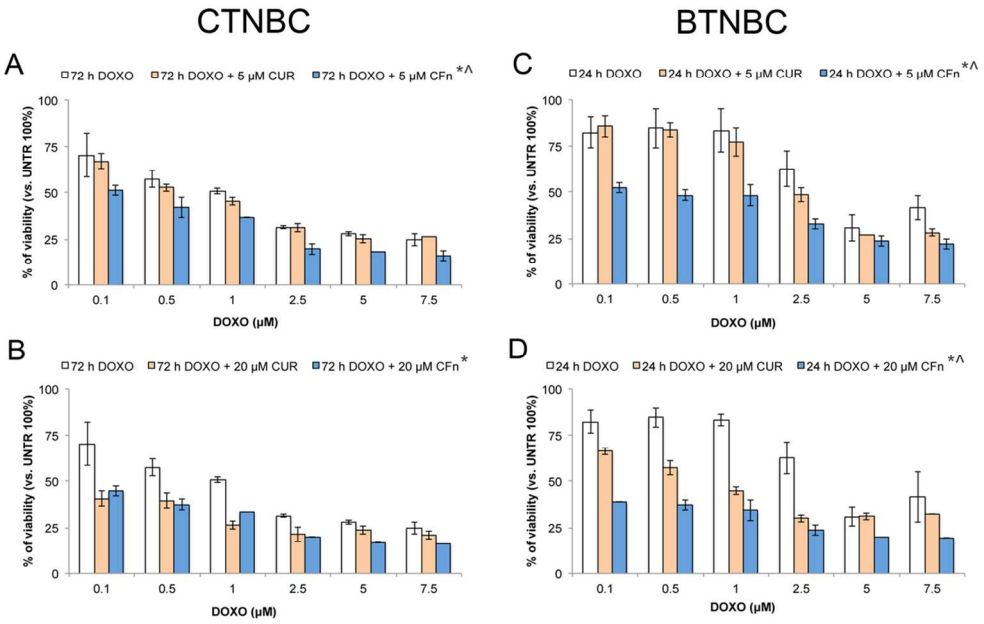

Figure 7. Sensitization of breast cancer cells to doxorubicin mediated by Cur or CFn. Treatment of CTNBC and BTNBC cells with different concentrations of Dox (from 0.1 to 7.5 μM) with the addition of 5 and 20 μM Cur or CFn up to 72 h for CTNBC cells (A, B) and 24 h for BTNBC (C, D). *P<0.05 vs. Dox; ^P<0.05 vs. Dox + Cur after one-way ANOVA analysis. All other treatment combinations are shown in Figure S7.

111x72mm (300 x 300 DPI)

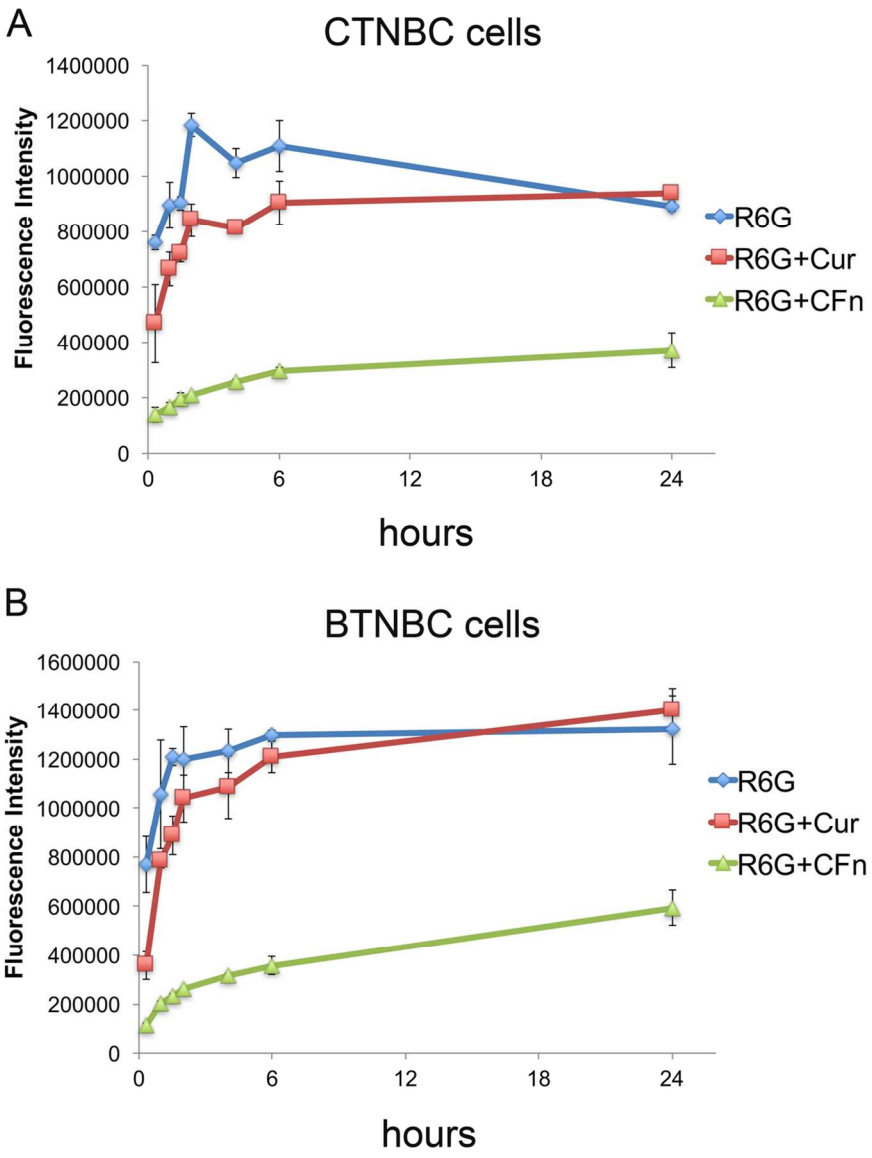

Figure 8. Inhibition of Rhodamine 6G efflux by TNBC cells. After treating BTNBC (A) and CNTBC cells (B) with 1 μg mL^{-1} R6G for 1 h at 37 °C, 20 μM Cur or CFn were added and the fluorescence intensity of R6G was read in the supernatants at different time points. Data represent mean of three replicates ± SD.

110x149mm (300 x 300 DPI)

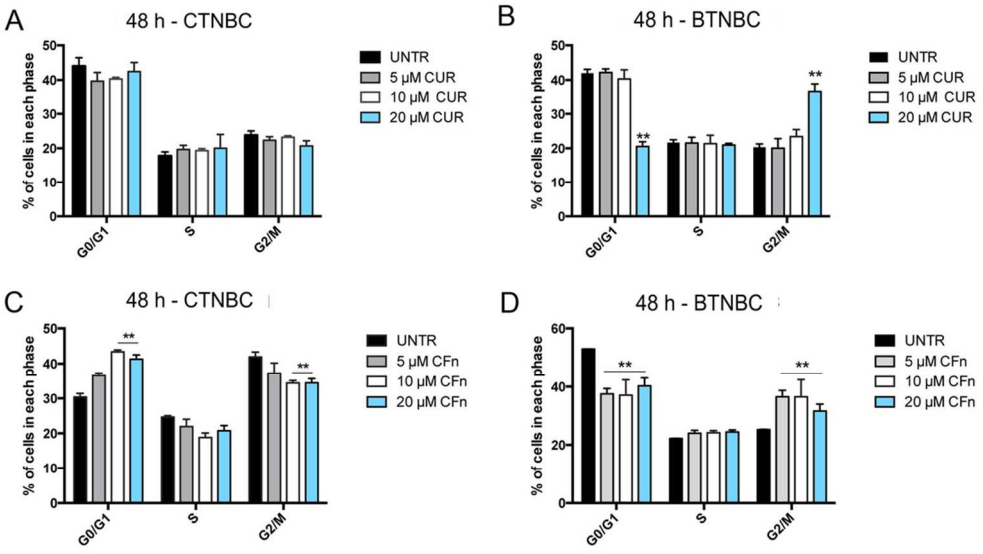

Figure 9. Cell cycle analysis of CTNBC and BTNBC cells treated with 5, 10 and 20 μM Cur and CFn up to 48 h. Cells were labeled with PI to determine the DNA content in each cell cycle phase by flow cytometry. Data represent the mean of percentage of cell distribution in each phase ± SD. **P<0.01 vs. UNTR after one-way ANOVA analysis.

99x57mm (300 x 300 DPI)

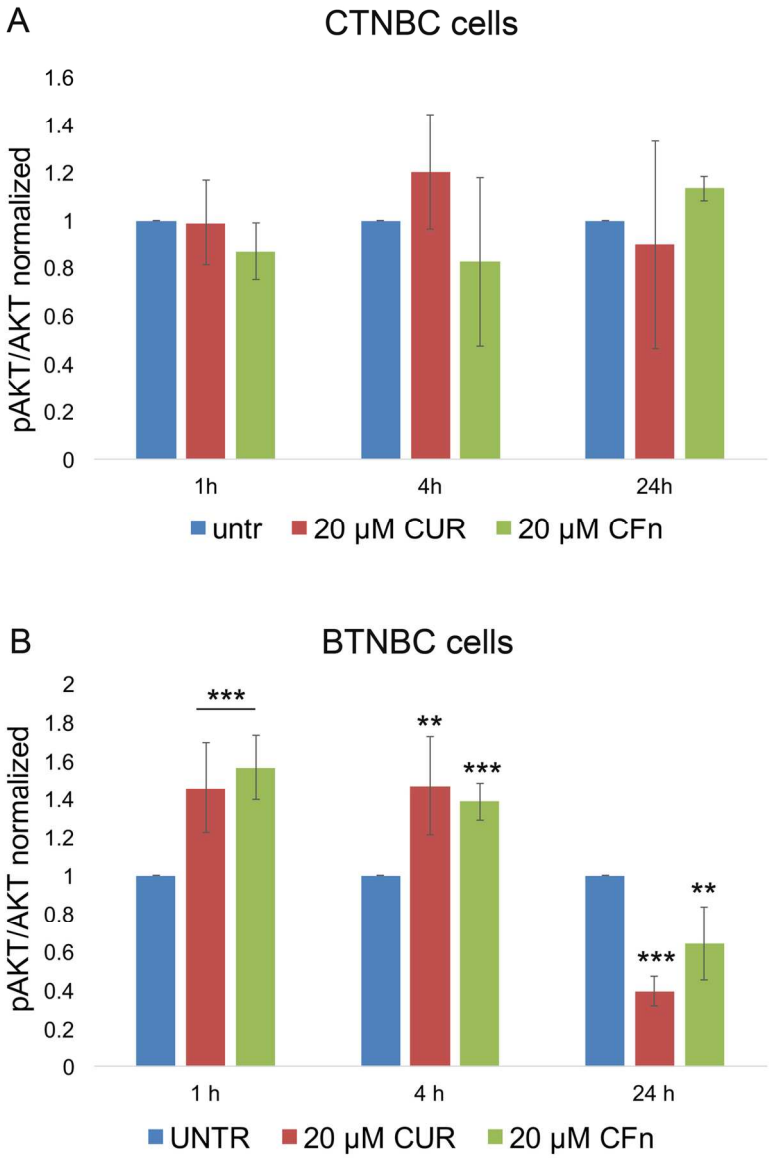

Figure 10. Analysis of p-Akt (Ser473) with Alpha technology. BTNBC (A) and CTNBC (B) cells were treated with 20 μM Cur or CFn for 1, 4 and 24 h. Alpha signals were read with Ensight multiplate reader (Perkin Elmer), normalized on Akt total signals and represented as mean ± SD. **P<0.05 vs. UNTR; ***P<0.01 vs. UNTR after one-way ANOVA analysis.

124x188mm (300 x 300 DPI)